Synthesis of weakly-agglomerated luminescent CaWO4:Nd3+ particles by modified Pechini method

Medvedev Vassily A., Shubina Irina M., Kolesnikov Ilya E., Lähderanta Erkki, Mikhailov Mikhail D., Manshina Alina A., Mamonova Daria V.

DOI: 10.1016/j.ceramint.2021.11.048

Synthesis of weakly-agglomerated luminescent $CaWO_4:Nd^{3+}$ particles by modified Pechini method

Vassily A. Medvedev[a], Irina M. Shubina[a], Ilya E. Kolesnikov[a,b], Erkki Lahderanta[b], Mikhail D. Mikhailov[c], Alina A. Manshina[a], Daria V. Mamonova[a]*

[a]Saint Petersburg State University, Saint Petersburg, 199034, Russia

[b] LUT University, Skinnarilankatu 34, 53850, Lappeenranta, Finland

[c]Peter the Great St.Petersburg Polytechnic University, Saint Petersburg, 194064, Russia

***Corresponding author: Phone: +7-812-4287479; E-mail: magwicher@gmail.com

Abstract:

The specific luminescence behavior of crystalline oxide particles doped with rare earth ions strongly depends on the initial composition of the host material and synthesis conditions. Especially with non-isovalent doping in the crystal lattice, when the formation of the structure is accompanied by the formation of point defects serving as charge compensators. The work is devoted to the synthesis of $CaWO_4:Nd^{3+}$ particles in the salt melt (modified Pechini method) and the research of structural and luminescent properties under varying synthesis conditions. Temperature and duration of heat treatment in the salt melt (KCl) affected the crystal structure, the size of coherent scattering regions, luminescence intensity, and lifetime. $CaWO_4:Nd^{3+}$ powders contain both coarse and fine fractions. Weak particle agglomeration makes it possible to get a water dispersion with individual nanoparticles. An increase of heat treatment temperature led to a reduction of luminescence intensity and lifetime due to the formation of point defects. From the luminescence properties point of view, the optimal synthesis conditions of $CaWO_4:Nd^{3+}$ crystalline particles in salt melt were T_1= 600 ºC; t_1=2 hours (the stage of polymer gel thermal treatment), T_2= 800 ºC; t_2=1 hour (the stage of thermal treatment in KCl salt melt). According to the obtained results, the synthesized material is potentially promising for use as fluorescent thermometers and biological labels.

Keywords: Powders: chemical preparation; Optical properties; Metal oxides

1. Introduction

One of the most promising luminophores doped with rare earth ions (REI) are metal oxides because of their thermal stability over a wide temperature range, chemical inertness, stability of optical and mechanical properties, and biocompatibility. The combination of these properties makes these materials interesting for use in instrumentation, display, sensor technology, and, of course, medical applications [1–4]. Functional properties and small particle size of the oxide luminophores are the most important parameters for the field of biomedicine (luminescent sensors, nanothermometers, etc.). The intensity of the luminescence is crucial and strongly dependent on the crystalline structure. Nanosized particles have a large surface area with a large accumulation of defects on which luminescence quenching can be observed [5]. High temperatures and heat treatment times reduce the defects and increase the coherent scattering region (CSR) size [6], which leads to an increase in the luminescence intensity. However, high-temperature processes also lead to agglomeration and sintering of particles. This is well demonstrated by methods such as solid-phase synthesis [7], mechanochemical synthesis [8], and deposition from aqueous solutions [9]. Weak agglomeration is observed in powders synthesized by hydrothermal synthesis [10], laser ablation [11], sonochemical method [12], and sol-gel synthesis [13]. In such a way, finding a balance between synthesis parameters for providing high CSR size and low particles agglomeration is a topical task for the creation of oxide higher-melting-point nanoparticles (NPs).

The samples presented in this work were synthesized with the modified Pechini method that has been proven to yield high quality crystalline particles of $Y_3Al_5O_{12}$, YVO_4, $MgAlO_4$, $Lu_2(WO_4)_3$ doped with various REI [5,14–16]. This method is based on reactions between composite oxides in a high-temperature solvent - a salt melt [17]. A complex oxide is formed during the calcination of a mixture of simple oxides and the resulting sample consists of product particles distributed in a solid salt matrix after cooling. The water-soluble salt is easily removed from the system and results in weakly agglomerated

particles. In the modified Pechini method it is proposed to repeat the heat treatment. Complex oxide particles, amorphous or crystalline, are first obtained at low temperatures when sintering, crystal growth and agglomeration processes are not intensive. A heat treatment in salt melt then follows. Repeat heat treatment in salt melt prevents sintering of particles, and high temperatures promote further crystallization processes and growth of CSR [14]. Therefore, the method combines a high temperature to form a crystalline structure and a solvent to reduce agglomeration.

REI-doped $CaWO_4$ is an optical material with a scheelite structure. It is important for applications in many fields such as lasers, fluorescent lamps, scintillators, quantum electronics, thermometry and white light-emitting diodes [18–22]. These particles have not been synthesized with the modified Pechini method before. The specific luminescence behavior of crystalline particles is highly sensitive to the initial composition of the host material, doping concentration and synthesis conditions. The work investigates the parameters of synthesis in salt melt and their influence on the crystal structure, morphology (size and agglomeration) and luminescence properties of $CaWO_4:Nd^{3+}$ particles. The effect of the type of solvent on the structure and luminescence properties of the particles is demonstrated for the first time. KCl and Na_2SO_4 salts were used as high-temperature solvents.

2. Experimental section

Complex oxide samples were obtained using the modified Pechini method [14]. Basic starting reagents for $CaWO_4:Nd^{3+}$ synthesis are Nd_2O_3 (99.99 %), $Ca(NO_3)_2 \cdot 4H_2O$ (99.0 %) and ammonium paratungstate $(NH_4)_{10}(H_2W_{12}O_{42}) \cdot 4H_2O$ (99.0 %). The neodymium oxide is converted to nitrate by the addition of concentrated nitric acid:

$$Nd_2O_3 + 6\,HNO_3 = 2\,Nd(NO_3)_3 + 3\,H_2O \quad (1)$$

Calcium nitrate and ammonium paratungstate are dissolved apart in distilled water. A saturated water citric acid solution was added to the metal nitrates and ammonium paratungstate in a volume ratio of 1/1 for complex formation:

$$Nd(NO_3)_3 + 3C_6H_8O_7 = [Nd(C_6H_8O_7)_3](NO_3)_3 \quad (2)$$

$$Ca(NO_3)_2 + 3C_6H_8O_7 = [Ca(C_6H_8O_7)_3](NO_3)_2 \quad (3)$$

$$(NH_4)_{10}(H_2W_{12}O_{42}) + 24H_3cit + 12OH^- \rightarrow 12[WO_3(H_2cit)_2\,OH]^{3-} + 10NH_4^+ + 6H_2O + 14H^+ \quad (4)$$

Citric acid plays the role of a chelating agent for metal ions. The metal citrate complexes are then mixed. Then the esterification reaction was carried out. Ethylene glycol was used for cross-linking in a polymer. The reagent mixture was kept at 70 ºC for 10 hours. This part of the synthesis refers to the standard Pechini synthesis [6,23]. The gel was calcined in two stages. The first stage at T_1=600 °C for t_1 = 2 hours is to remove organic compounds. Then powder was co-dispersed with potassium chloride or sodium sulfate in a mass ratio 1:1. The second heat treatment stage was carried out in salt melt at T_2 = 800, 900, 1000 and 1100 °C for t_2 = 0,5 - 3 hours for KCl and T_2 = 1000 °C, t_2 = 1 hour for Na_2SO_4. Salt was removed from the product by washing in distilled water. $CaWO_4$ and $CaWO_4:Nd^{3+}$ (0,5 at.%) samples were obtained using the method described. The synthesis steps are shown in the diagram (Fig. 1).

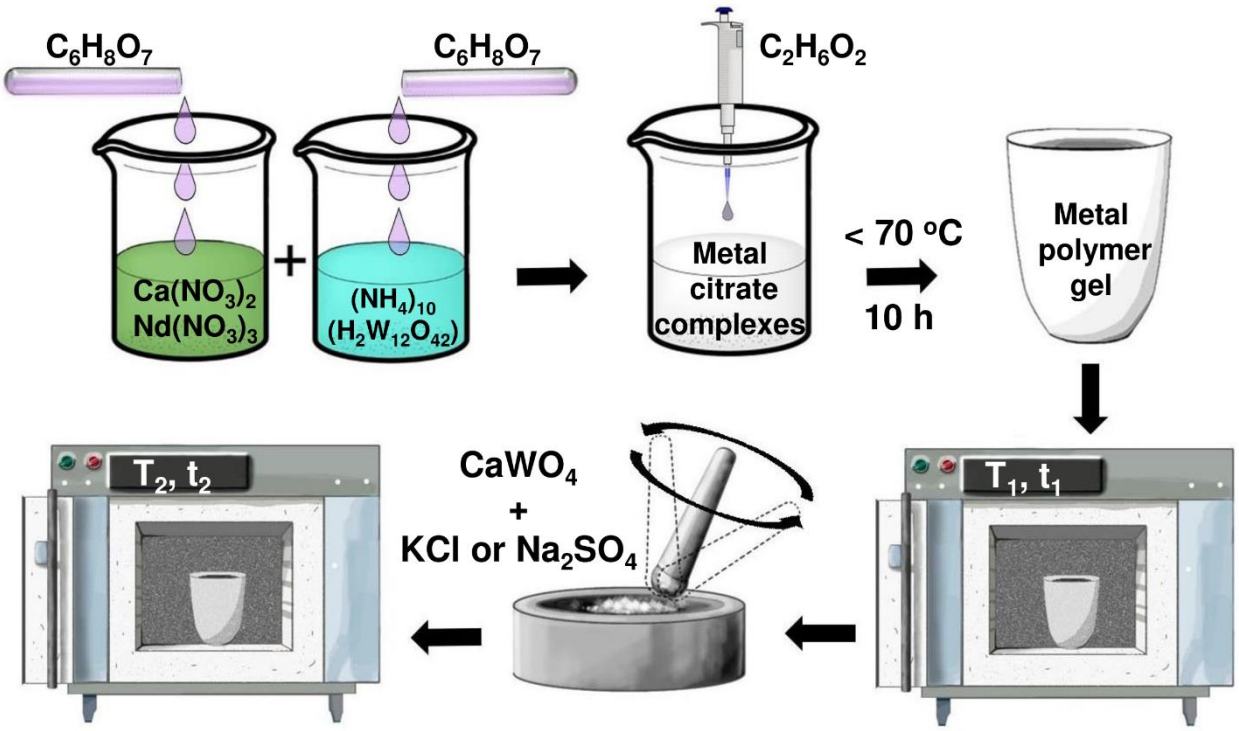

Fig. 1. Synthesis diagram of modified Pechini method for $CaWO_4:Nd^{3+}$ powder.

Thermogravimetric analysis of metal-polymer gel in an oxygen-containing environment has been done in the temperature range from 40 to 1200 °C with NETZSCH TG 209 F1 Libra Thermogravimetric Analyzer. Scanning electron microscopy was used to characterize morphology with Zeiss Supra 40VP microscope. The static light scattering method provided a size distribution curve of the particles in the water solution (laser granulometer Mastersizer 3000). The powder was dispersed by Hielscher UP400St Ultrasonic Processor in distilled water (400 W, frequency 24 kHz) to obtain this solution. X-Ray Diffraction (XRD) patterns were measured with the research facility Bruker "D8 DISCOVER" with CuKα. Information about crystal unit cell parameters and the size of CSR have been calculated using TOPAS software. Size of CSR was obtained through full-profile analysis of XRD patterns by the Rietveld method. Photoluminescence properties were studied with modular spectrofluorimeter Fluorolog-3 equipped with Xe-arc lamp (450 W power).

3. Results and discussions

The Thermogravimetric (TG) and Differential Scanning Calorimeter (DSC) analysis curves demonstrate the mass reduction and heat flow change during the heat treatment of the metal-polymer gel (Fig. 2.a). In the temperature range of 400 - 600 °C an endothermic reaction (pyrolysis of polymer gel and reaction of simple CaO and WO_3 oxides) takes place and the mass is decreasing by 54 %. Calcium and tungsten oxides remain in the system and form a complex tungsten oxide structure after the first heat treatment (T_1= 600 °C; t_1=2 h). This powder contains mainly tetragonal phase $CaWO_4$ and a small number of monoclinic Ca_3WO_6 according to XRD results. The second stage of thermal treatment in a salt melt produces a single-phase crystalline $CaWO_4$ powder. The diffraction lines for samples synthesized in KCl and Na_2SO_4 melts are narrower, indicating that the defects in the crystalline particles are reduced for both salts in comparison with a single-stage process (Fig. 2b). The heat treatment into salt melt allows increasing the average CSR size of up to 200 nm. CSR was found to be about 100 nm for Na_2SO_4 and over 150 nm for KCl, while the CSR sizes don't exceed 25 nm without salt. The unit cell parameters for all the samples are 312.8 $Å^3$. To determine the optimal conditions for the second heat treatment (temperature T_2 and time t_2) KCl was used, because the growth of the CSR is more efficient in this case.

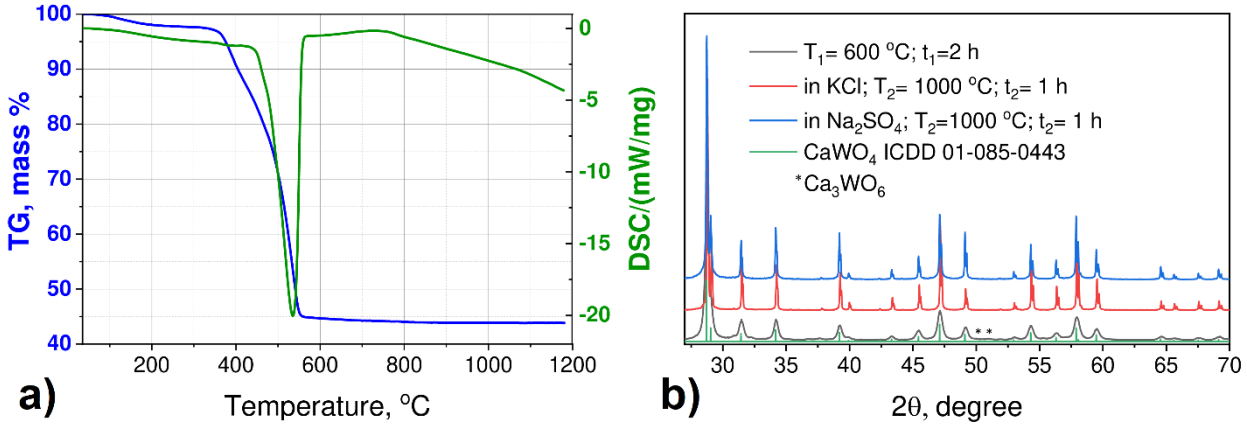

Fig. 2. a) TG-DSC curves of particle formation process from metal-polymer gel to $CaWO_4$ phase formation; b) XRD results for different synthesis conditions of samples and standard card of $CaWO_4$ ICDD 01-085-0443.

Investigation of the structure of a series of $CaWO_4:Nd^{3+}$ (0,5 at.%) samples with T_2=800, 900, 1000, 1100 °C (t_2=1 h) shows changes in the average size of CSR from 150 nm to 200 nm with temperature increasing. With increase of time t_2 up to 3 h this parameter reaches 265 nm.

A significant change in the morphology of the powders is observed with an increase in the calcination temperature. Fig. 3 shows the results of SEM for the particles after the first stage of heat treatment and after the second stage in KCl. The large agglomerates are irregularly shaped in Fig. 3a. At higher resolution (Fig. 3 b) it is difficult to see the boundaries of the individual particles, indicating agglomerating and fritting. There is considerable particle growth after the second stage of heat treatment (Fig. 3c). The particles smaller than 200 nm cover the surface of large particles up to 10 μm with planes (Fig. 3d). The SEM results are in agreement with the particle size distribution obtained from the statistical light scattering technique (SLS). After ultrasonic dispersion of the powder in water the solution contains a fine particle fraction up to 200 nm, and a coarse particle fraction with sizes from 1 to 10 μm (Fig. 3e).

When T_2 temperature is increased to 1100 °C, the aggregates reach tens of microns in size (Fig. 4 c). These sizes are an order of magnitude higher than at 800 °C (Fig. 4 a,b). The particles lose their planes and a layer of nanoparticles can be observed on the surface (Fig. 4d).

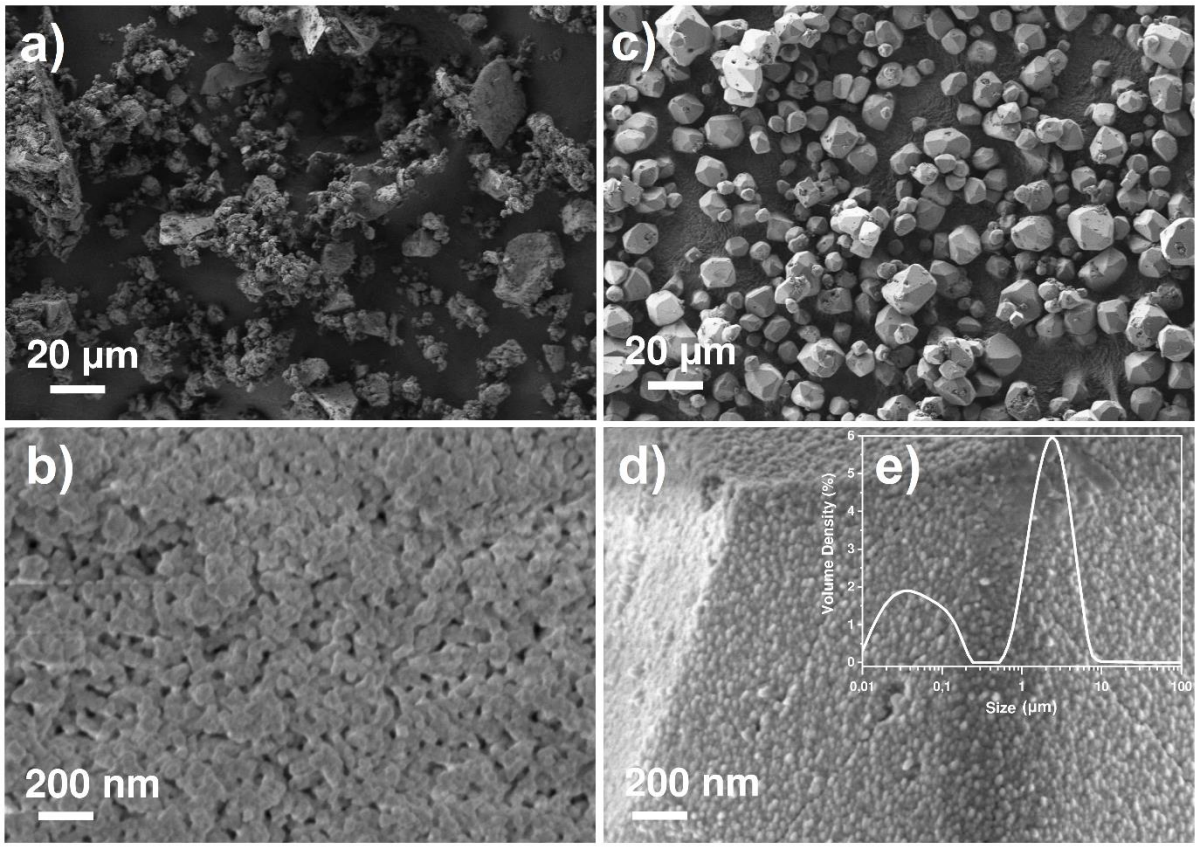

Fig. 3. SEM images of $CaWO_4:Nd^{3+}$ 0.5 at.% particles: a) and b) after first heat treatment stage (T_1= 600 °C; t_1=2 h); c) and d) after second heat treatment stage in KCl (T_2= 900 °C; t_2=1 h); e) Size distribution of $CaWO_4:Nd^{3+}$ 0.5 at.% colloidal solution.

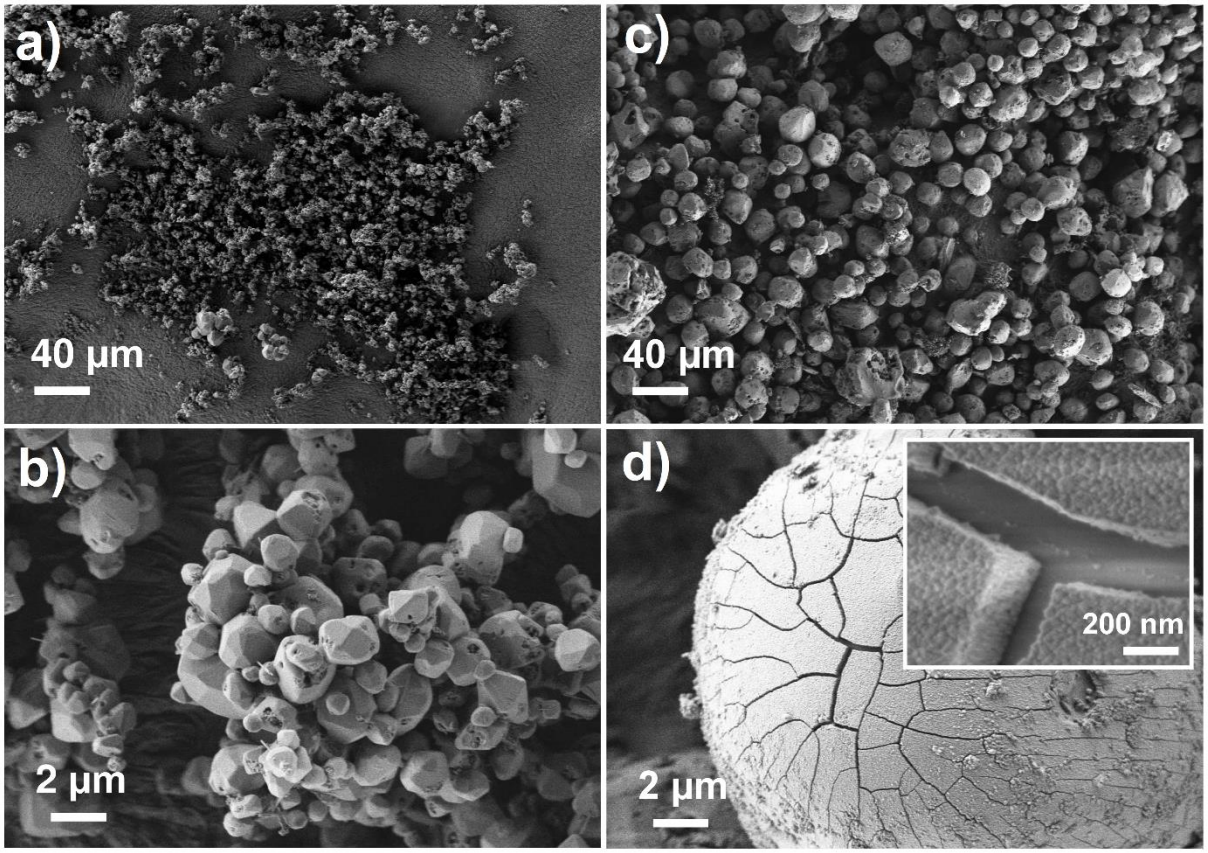

Fig. 4. SEM images of $CaWO_4:Nd^{3+}$ 0.5 at.% particles after treatment in KCl a), b) T_2= 800 °C; t_2=1 h; c), d) T_2= 1100 °C; t_2=1 h.

Luminescence properties of $CaWO_4$ sample and $CaWO_4:Nd^{3+}$ 0.5 at.% series with different synthesis conditions were studied. The undoped $CaWO_4$ crystalline host has emission band centered at about 398 nm when excited at λ_{ex}=250 nm (Fig. 5a). Emission spectrum of $CaWO_4:Nd^{3+}$ 0.5 at.% sample measured upon 587 nm excitation consists of typical intraconfigurational transitions inside Nd^{3+} ions: $^4F_{5/2} - {}^4I_{9/2}$ (810 nm), $^4F_{3/2} - {}^4I_{9/2}$ (882 nm), $^4F_{3/2} - {}^4I_{11/2}$ (1066 nm), and $^4F_{3/2} - {}^4I_{13/2}$ (1337 and 1382 nm) (Fig. 5b).

Excitation spectra of undoped and doped with Nd^{3+} ions $CaWO_4$ samples are shown in Fig. 5c. One can see the red shift of $CaWO_4$ host absorption with the introduction of rare earth ions in the crystalline host. This effect is probably related to the formation of new energy levels due to the structure distortion (defect formation) associated with by non-isovalent substitution of Ca^{2+} by Nd^{3+} [24,25]. Noteworthy, the aforementioned red shift was observed in both cases of host (398 nm) and Nd^{3+} (1066 nm) luminescence.

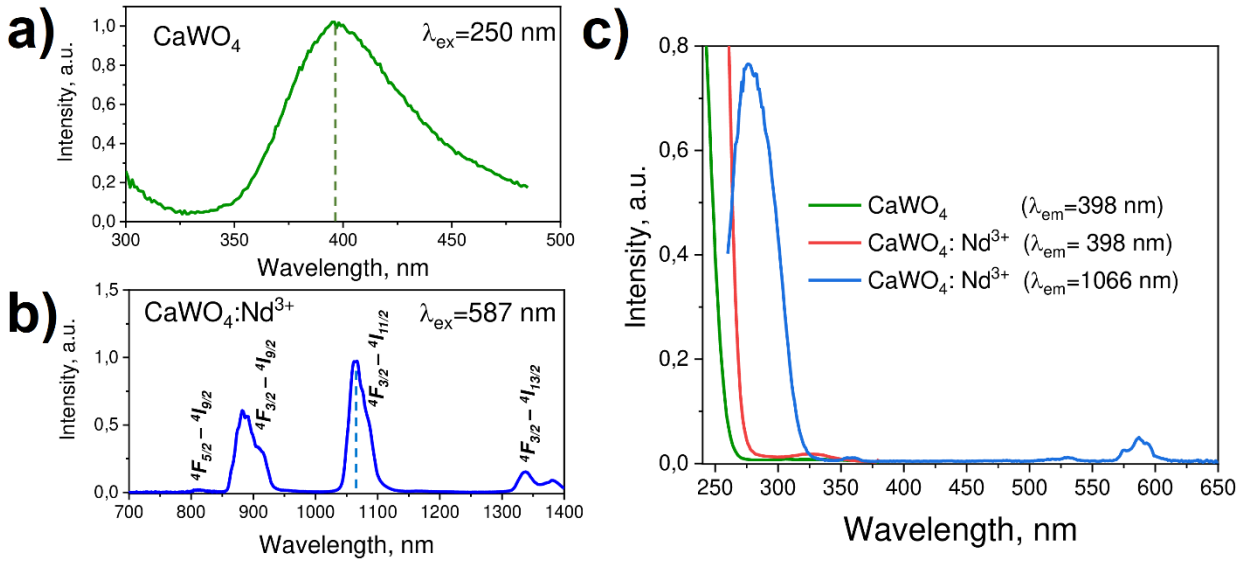

Fig. 5. a) Emission spectrum of $CaWO_4$ sample upon λ_{ex}=250 nm; b) emission spectrum of $CaWO_4:Nd^{3+}$ (0.5 at.%) sample upon λ_{ex}=587 nm; c) excitation spectra of $CaWO_4$ and $CaWO_4:Nd^{3+}$ (0.5 at.%) samples.

As the solubility of the oxides in the salt melt for heat treatment depends on its composition, $CaWO_4$ Nd^{3+} 0.5 at.% powder was synthesized in KCl and Na_2SO_4 melts for comparison. Fig. 6 shows the excitation and emission spectra of samples synthesized in different melts as well as a sample after the first calcination (T_1= 600 °C; t_1=2 h).

One can see that positions of excitation and emission bands do not depend on the particular salt melt used during the synthesis procedure. However, luminescence intensity was significantly affected by this parameter. Noteworthy, the sample without second calcination demonstrated more efficient luminescence in the case of direct excitation mechanism (through Nd^{3+} ions) (Fig. 6a). The most intense emission upon host excitation was observed for particles synthesized in the KCl (Fig. 6b).

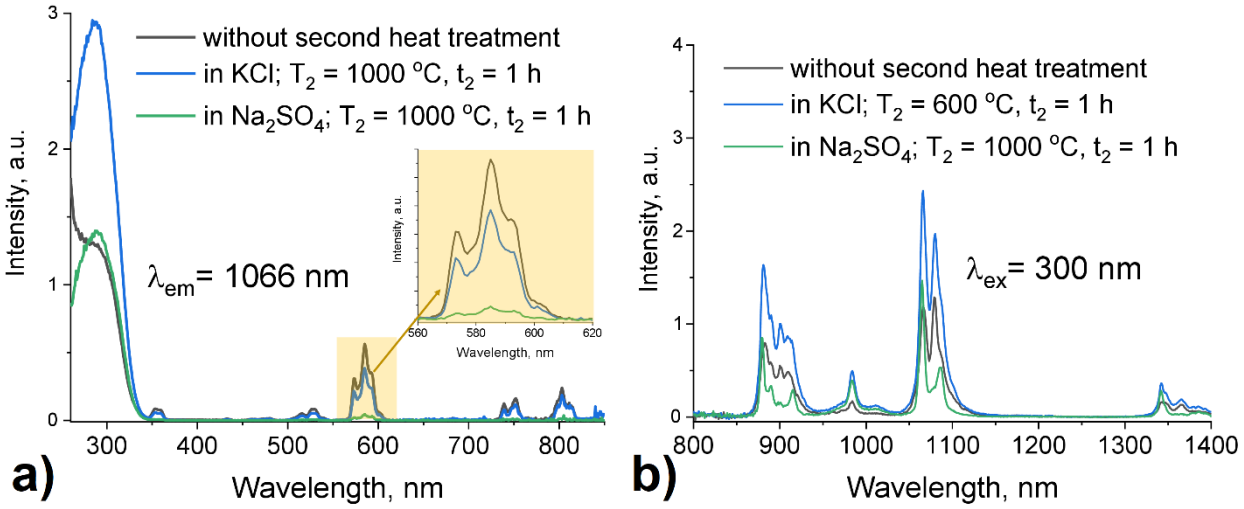

Fig. 6. a) Excitation and b) emission spectra of $CaWO_4:Nd^{3+}$ 0.5 at.% samples with different synthesis conditions.

Further, we studied the effect of synthesis conditions (temperature and duration of heat treatment) on luminescence properties of prepared $CaWO_4:Nd^{3+}$ 0.5 at.% samples. Excitation spectra of $CaWO_4:Nd^{3+}$ temperature series measured for the most prominent $^4F_{3/2} - {}^4I_{11/2}$ (1066 nm) transition are presented in Fig. 7a. The second calcination temperature was varied from 800 °C to 1100 °C. The obtained spectra include strong wide band at 290 nm attributed to excitation via crystalline host and low intensity peaks in the longer wavelength region corresponding to Nd^{3+} transitions: $^4I_{9/2} - {}^4D_{3/2} + {}^4D_{1/2}$ (355 nm), $^4I_{9/2} - {}^4G_{7/2} + {}^4G_{9/2} + {}^2K_{13/2}$ (515 and 528 nm), $^4I_{9/2} - {}^4G_{5/2} + {}^4G_{7/2} + {}^2H_{11/2}$ (574, 585 and 593 nm), $^4I_{9/2} - {}^4F_{7/2} + {}^4S_{3/2}$ (739 and 752 nm), $^4I_{9/2} - {}^4F_{5/2} + {}^4H_{9/2}$ (803 nm) [26,27]. Noteworthy, temperature increase leads to the reduction of excitation efficiency through the crystalline host, while direct excitation mechanism does not show significant change. The observed behavior can be explained by an increase in point defects serving as charge compensators in the crystalline structure along with calcination temperature increase [28,29]. Synthesis time with T_2 = 800 °C did not affect the excitation efficiency in both cases: for excitation through the crystalline host and for direct excitation of neodymium ions (Fig. 7b).

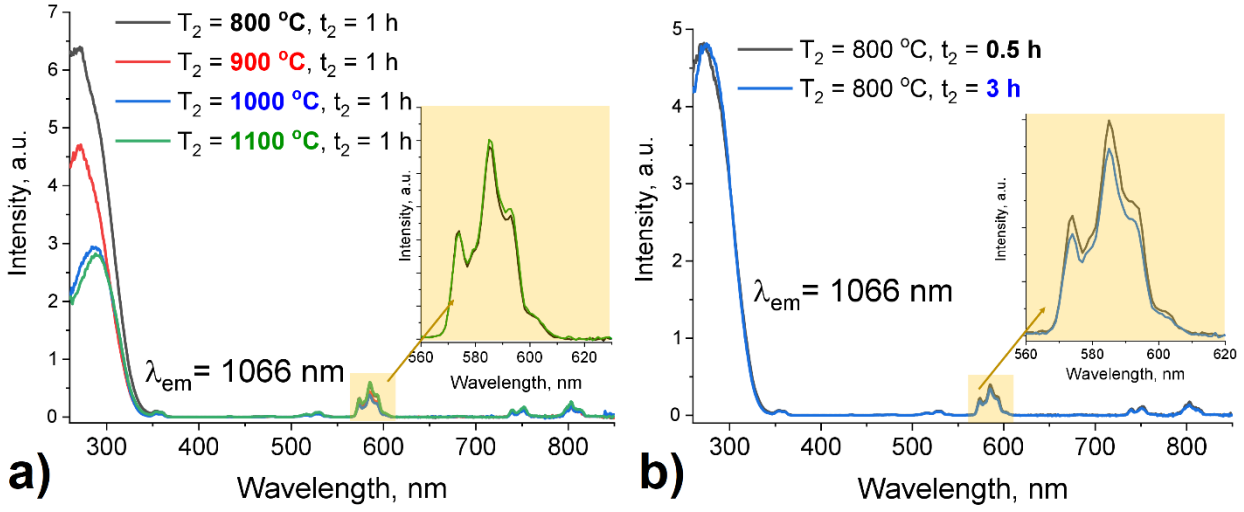

Fig. 7. Excitation spectra of $CaWO_4:Nd^{3+}$ 0.5 at.% samples synthesized in KCl with a) different T_2 (800 – 1100 °C) and b) different t_2 (0.5 and 3 h).

Emission spectra of $CaWO_4:Nd^{3+}$ temperature series were measured using two excitation mechanisms: 1) excitation through the crystalline host λ_{ex}=300 nm; 2) direct excitation of Nd^{3+} ions at λ_{ex}=585 nm. One can see a monotonic decrease of emission intensity along with an increase of second calcination temperature (Fig. 8a). Emission spectra obtained upon direct excitation also revealed such behavior, but intensity reduction was much less than in the case of host doping (Fig. 8b).

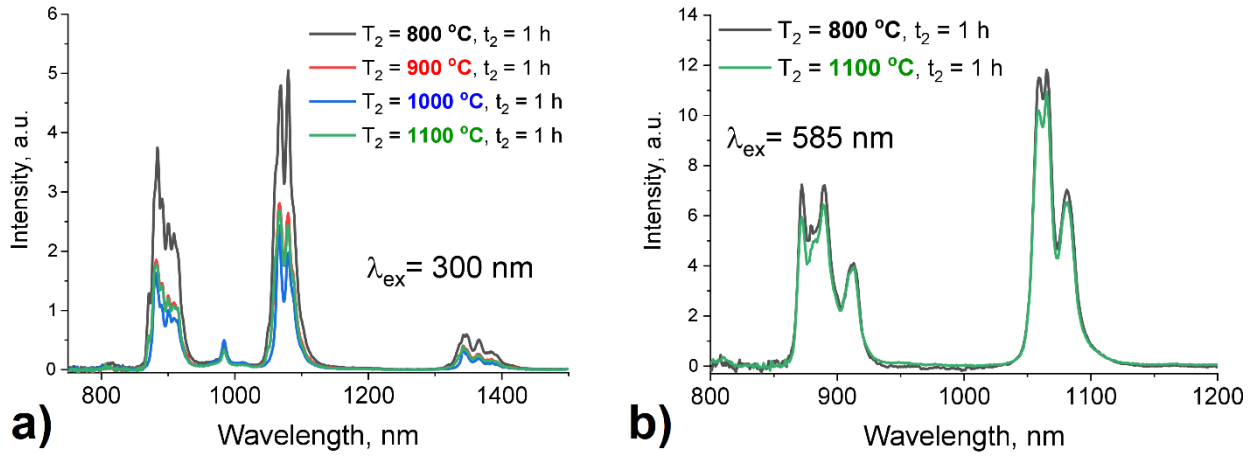

Fig. 8. Emission spectra of $CaWO_4:Nd^{3+}$ 0.5 at.% temperature series synthesized in KCl with different T_2 upon a) host excitation (λ_{ex}=300 nm); b) Nd^{3+} ions direct excitation (λ_{ex}=585 nm).

Fig. 9 demonstrates luminescence kinetics decays for $CaWO_4:Nd^{3+}$ 0.5 at.% temperature and time series. Decay curves were monitored for the most intense transition $^4F_{3/2} - {}^4I_{11/2}$ (1066 nm) of Nd^{3+} ions upon host excitation (λ_{ex}=300 nm). As it can be seen, all experimental data showed mono-exponential behavior and were fitted with the following formula: $I = I_0 \cdot e^{-\frac{t}{\tau_f}}$, where τ_f is the observed lifetime of $^4F_{3/2}$ level. The observed lifetime monotonically decreases from 139 to 110 μs along with the increase of calcination temperature T_2 (inset of Fig. 9a). Growth of calcination duration in the salt melt also resulted in an insignificant lifetime decrease (Fig. 9b).

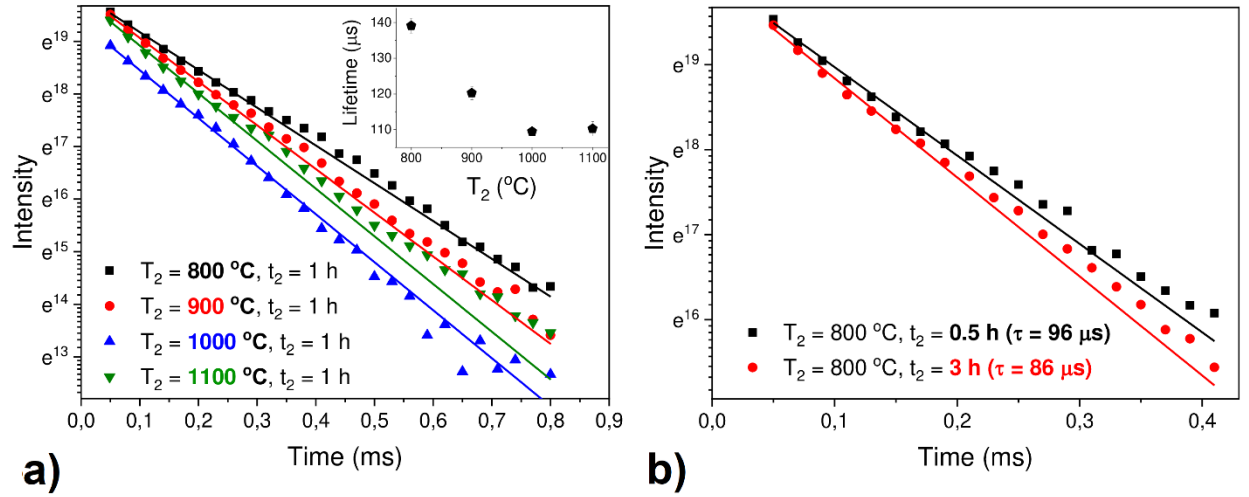

Fig. 9. Luminescence decays of $CaWO_4:Nd^{3+}$ (0.5 at.%) synthesized in salt melt (T_1=600 °C; t_2= 2 h): a) T_2 temperature series; b) t_2 time series. Inset: $^4F_{3/2}$ level lifetime.

4. Conclusion

Nd^{3+}-doped $CaWO_4$ powders were synthesized using the modified Pechini method. The prepared samples showed a pure crystalline phase without any structural impurity. Second heat treatment in salt melt resulted in increase of CRS and particle size compared to the standard Pechini technique. The increase of temperature and duration of this heat treatment also led to the increase of CRS (from 150 to 200 nm). According to SEM and SLS results, powders consist of micro- (1-10 μm) and nanoparticles (up to 200 nm), from which the water dispersion can be obtained. Emission and excitation spectra of undoped and Nd^{3+}-doped $CaWO_4$ samples were measured. Red shift of the host excitation band was observed in both cases of host (398 nm) and Nd^{3+} (1066 nm) luminescence, which is explained by the formation of new energy levels due to the structure distortion. Emission spectra included typical 4f-4f transitions from $^4F_{5/2}$ and $^4F_{3/2}$ excited to lower levels. Using of KCl as the salt melt allowed obtaining higher emission

intensity of $CaWO_4:Nd^{3+}$ compared to Na_2SO_4. Growth of temperature of heat treatment in salt melt resulted in the decrease of excitation efficiency through the crystalline host, while Nd^{3+} direct excitation mechanism was kept unchanged. Duration of heat treatment with T_2 = 800 °C did not affect the excitation efficiency for excitation mechanisms. All luminescence decay curves of $CaWO_4:Nd^{3+}$ measured for intense $^4F_{3/2}$ – $^4I_{11/2}$ transition (1066 nm) displayed mono-exponential behavior. $^4F_{3/2}$ lifetime monotonically decreased along with an increase of calcination temperature T_2 (from 139 to 110 μs) and calcination duration in the salt melt (from 96 to 86 μs). Based on the obtained results, the optimal conditions of synthesis of $CaWO_4:Nd^{3+}$ crystalline particles in salt melt were determined to be T_1= 600 °C; t_1=2 hours (the stage of polymer gel thermal treatment), T_2= 800 °C; t_2=1 hour (the stage of thermal treatment in salt melt, KCl).

Acknowledgments

Authors are grateful to “Interdisciplinary Resource Centre for Nanotechnology”, Resource Center "Innovative technologies of composite nanomaterials”, “Thermogravimetric and Calorimetric Research Centre”, “Centre for Geo-Environmental Research and Modelling (GEOMODEL)”, “Research Centre for X-ray Diffraction Studies” and “Centre for Optical and Laser Materials Research” of Saint-Petersburg State University Research Park. The authors are grateful to "Russian president grant" No. MK-1306.2020.3

References

[1] J.B. Prasanna kumar, G. Ramgopal, Y.S. Vidya, K.S. Anantharaju, B. Daruka Prasad, S.C. Sharma, S.C. Prashantha, H.B. Premkumar, H. Nagabhushana, Bio-inspired synthesis of Y2O3: Eu3+ red nanophosphor for eco-friendly photocatalysis, Spectrochimica Acta Part A: Molecular and Biomolecular Spectroscopy. 141 (2015) 149–160. https://doi.org/10.1016/j.saa.2015.01.055.

[2] S.E. Crawford, P.R. Ohodnicki, J.P. Baltrus, Materials for the photoluminescent sensing of rare earth elements: challenges and opportunities, J. Mater. Chem. C. 8 (2020) 7975–8006. https://doi.org/10.1039/D0TC01939A.

[3] P.P. Paganini, L.A.O. Nunes, STUDY OF QUANTUM DOT BASED ON TIN/YTTRIUM MIXED OXIDE DOPED WITH TERBIUM TO BE USED AS BIOMARKER, (2009) 8.

[4] A.P. Patel, C.R. Schorr, D. Viswanath, K. Sarkar, N.J. Streb, V.J. Pizzuti, R. Misra, J. Lee, Y.-Y. Won, Pilot-Scale Optimization of the Solvent Exchange Production and Lyophilization Processing of PEG–PLA Block Copolymer-Encapsulated $CaWO_4$ Radioluminescent Nanoparticles for Theranostic Applications, Ind. Eng. Chem. Res. 60 (2021) 7081–7096. https://doi.org/10.1021/acs.iecr.0c05852.

[5] E.V. Golyeva, D.V. Tolstikova, I.E. Kolesnikov, M.D. Mikhailov, Effect of synthesis conditions and surrounding medium on luminescence properties of YVO4:Eu3+ nanopowders, Journal of Rare Earths. 33 (2015) 129–134. https://doi.org/10.1016/S1002-0721(14)60392-6.

[6] D.V. Mamonova, M.D. Mikhailov, K.G. Sevast’yanova, A.V. Semencha, A.S. Tver’yanovich, A.L. Shakhmin, Synthesis of nanocrystalline powders of yttrium aluminum garnet doped by neodymium, Nanotechnol Russia. 6 (2011) 504–509. https://doi.org/10.1134/S1995078011040094.

[7] X. Wang, Y. Zhang, C. Hao, F. Feng, H. Yin, N. Si, Solid-Phase Synthesis of Mesoporous ZnO Using Lignin-Amine Template and Its Photocatalytic Properties, Ind. Eng. Chem. Res. 53 (2014) 6585–6592. https://doi.org/10.1021/ie404179f.

[8] T.J. Clarke, T.E. Davies, S.A. Kondrat, S.H. Taylor, Mechanochemical synthesis of copper manganese oxide for the ambient temperature oxidation of carbon monoxide, Applied Catalysis B: Environmental. 165 (2015) 222–231. https://doi.org/10.1016/j.apcatb.2014.09.070.

[9] J. Šubrt, V. Štengl, S. Bakardjieva, L. Szatmary, Synthesis of spherical metal oxide particles using homogeneous precipitation of aqueous solutions of metal sulfates with urea, Powder Technology. 169 (2006) 33–40. https://doi.org/10.1016/j.powtec.2006.07.009.

[10] P. Suneeta, R.A. Kumar, M.V. Ramana, G.K. Kumar, A. Chatterjee, C. Rajesh, Synthesis and optical properties of Mn-doped $CaWO_4$ nanoparticles, Phys. Scr. 95 (2020) 035806. https://doi.org/10.1088/1402-4896/ab4d2a.

[11] M. Kim, S. Osone, T. Kim, H. Higashi, T. Seto, Synthesis of Nanoparticles by Laser Ablation: A Review, KONA. 34 (2017) 80–90. https://doi.org/10.14356/kona.2017009.
[12] N.F. Andrade Neto, J.M.P. Silva, R.L. Tranquilin, E. Longo, J.F.M. Domenegueti, M.R.D. Bomio, F.V. Motta, Photoluminescent properties of Sm3+ and Tb3+ codoped CaWO4 nanoparticles obtained by a one-step sonochemical method, J Mater Sci: Mater Electron. 31 (2020) 13261–13272. https://doi.org/10.1007/s10854-020-03878-7.
[13] Z. Sun, L. Jiang, X. Xu, J. Li, X. Chen, H. Chen, Synthesis and Luminescence Properties of Ho3+ and Er3+-Doped CaWO4 Nanocrystalline Powders Prepared by Self-Propagating Combustion Method, J Fluoresc. 30 (2020) 389–396. https://doi.org/10.1007/s10895-020-02507-0.
[14] D.V. Mamonova, I.E. Kolesnikov, A.A. Manshina, M.D. Mikhailov, V.M. Smirnov, Modified Pechini method for the synthesis of weakly-agglomerated nanocrystalline yttrium aluminum garnet (YAG) powders, Materials Chemistry and Physics. 189 (2017) 245–251. https://doi.org/10.1016/j.matchemphys.2016.12.025.
[15] E.V. Golyeva, E.I. Vaishlia, M.A. Kurochkin, E.Y. Kolesnikov, E. Lähderanta, A.V. Semencha, I.E. Kolesnikov, Nd3+ concentration effect on luminescent properties of MgAl2O4 nanopowders synthesized by modified Pechini method, Journal of Solid State Chemistry. 289 (2020) 121486. https://doi.org/10.1016/j.jssc.2020.121486.
[16] E.V. Afanaseva, E.I. Vaishlia, E. Lähderanta, I.E. Kolesnikov, Synthesis and study of upconversion Lu2(WO4)3: Yb3+, Tm3+ nanoparticles synthesized by modified Pechini method, Optical Materials. 117 (2021) 111179. https://doi.org/10.1016/j.optmat.2021.111179.
[17] T.-S. Chin, S.L. Hsu, M.C. Deng, Barium ferrite particulates prepared by a salt-melt method, Journal of Magnetism and Magnetic Materials. 120 (1993) 64–68. https://doi.org/10.1016/0304-8853(93)91288-I.
[18] A. Golubović, R. Gajić, Z. Dohčević-Mitrović, S. Nikolić, Nd induced changes in IR spectra of CaWO4 single crystals, Journal of Alloys and Compounds. 415 (2006) 16–22. https://doi.org/10.1016/j.jallcom.2005.07.056.
[19] J. Liao, B. Qiu, H. Wen, W. You, Photoluminescence green in microspheres of CaWO4:Tb3+ processed in conventional hydrothermal, Optical Materials. 31 (2009) 1513–1516. https://doi.org/10.1016/j.optmat.2009.02.014.
[20] Yu.G. Zdesenko, F.T. Avignone III, V.B. Brudanin, F.A. Danevich, S.S. Nagorny, I.M. Solsky, V.I. Tretyak, Scintillation properties and radioactive contamination of CaWO4 crystal scintillators, Nuclear Instruments and Methods in Physics Research Section A: Accelerators, Spectrometers, Detectors and Associated Equipment. 538 (2005) 657–667. https://doi.org/10.1016/j.nima.2004.09.030.
[21] R.X. Wang, X.B. Luo, Luminescent Properties and Thermometry of $CaWO_4$:Nd^{3+} in Near Infrared Region, MSF. 893 (2017) 156–160. https://doi.org/10.4028/www.scientific.net/MSF.893.156.
[22] P.V. Ramakrishna, T. Lakshmana Rao, A. Singh, B. Benarji, S. Dash, Structural and photoluminescence behavior of thermally stable Eu 3+ activated CaWO 4 nanophosphors via Li + incorporation, Journal of Molecular Structure. 1149 (2017) 426–431. https://doi.org/10.1016/j.molstruc.2017.07.076.
[23] I.E. Kolesnikov, A.V. Povolotskiy, D.V. Tolstikova, A.A. Manshina, M.D. Mikhailov, Luminescence of $Y_3Al_5O_{12}$:Eu^{3+} nanophosphors in blood and organic media, J. Phys. D: Appl. Phys. 48 (2015) 075401. https://doi.org/10.1088/0022-3727/48/7/075401.
[24] D. Das, S.K. Gupta, C.S. Datrik, P. Nandi, K. Sudarshan, Role of alkali charge compensation in the luminescence of $CaWO_4$:Nd^{3+} and $SrWO_4$:Nd^{3+} Scheelites, New J. Chem. 44 (2020) 7300–7309. https://doi.org/10.1039/D0NJ00651C.
[25] V.V. Samartsev, R.G. Usmanov, I.Kh. Khadiev, E.F. Kustov, M.N. Baranov, Photon Echo in CaWO4:Nd3+ and LiAl5O8: Cr3+, phys. stat. sol. (b). 76 (1976) 55–66. https://doi.org/10.1002/pssb.2220760105.
[26] I.E. Kolesnikov, M.A. Kurochkin, A.A. Kalinichev, D.V. Mamonova, E.Yu. Kolesnikov, A.V. Kurochkin, E. Lähderanta, M.D. Mikhailov, Effect of silica coating on luminescence and temperature sensing properties of Nd3+ doped nanoparticles, Journal of Alloys and Compounds. 734 (2018) 136–143. https://doi.org/10.1016/j.jallcom.2017.11.048.
[27] I.E. Kolesnikov, D.V. Mamonova, E. Lähderanta, E.Y. Kolesnikov, A.V. Kurochkin, M.D. Mikhailov, Synthesis and characterization of Y2O3:Nd3+ nanocrystalline powders and ceramics, Optical Materials. 75 (2018) 680–685. https://doi.org/10.1016/j.optmat.2017.11.032.

[28] N. Suriyamurthy, B.S. Panigrahi, Investigations on luminescence of rare earths doped CaTiO3:Pr3+ phosphor, Journal of Rare Earths. 28 (2010) 488–492. https://doi.org/10.1016/S1002-0721(09)60138-1.
[29] A.A. Ryadun, E.N. Galashov, V.A. Nadolinny, V.N. Shlegel, ESR and luminescence of ZnWO4 crystals activated by gadolinium ions, J Struct Chem. 53 (2012) 685–689. https://doi.org/10.1134/S0022476612040105.